Inducing Magnetism in the Kondo Semiconductor CeRhSb through Hydrogenation: Antiferromagnetic Behavior of the New Hydride $CeRhSbH_{0.2}$

B. Chevalier,*,† R. Decourt,† B. Heying,‡ F. M. Schappacher,‡ U. Ch. Rodewald,‡ R.-D. Hoffmann,‡ R. Pöttgen,*,‡ R. Eger,§ and A. Simon*,§

Institut de Chimie de la Matière Condensée de Bordeaux (ICMCB), CNRS (UPR 9048), Université Bordeaux 1, 87 avenue du Docteur Albert Schweitzer, 33608 Pessac Cedex, France, Institut für Anorganische und Analytische Chemie, Universität Münster, Corrensstrasse 30, D-48149 Münster, Germany, and Max-Planck-Institut für Festkörperforschung, Heisenbergstrasse 1, D-70569 Stuttgart, Germany

Received September 12, 2006. Revised Manuscript Received October 12, 2006

CeRhSb was prepared from the elements by arc-melting. A single crystal of this antimonide was investigated on the basis of X-ray diffractometer data: TiNiSi type; *Pnma*; $a = 741.58(9)$, $b = 461.80(9)$, $c = 785.77(8)$ pm; wR2 = 0.0960; 645 F^2 values; 20 variable parameters. Hydrogenation leads to the formation of the new hydride $CeRhSbH_{0.2}$ which adopts the same structure but with a slightly larger unit cell volume: $a = 742.2(2)$, $b = 462.5(2)$, $c = 787.7(2)$ pm; wR2 = 0.1444; 443 F^2 values; 20 variable parameters. The rhodium and antimony atoms build up three-dimensional [RhSb] networks with Rh−Sb distances ranging from 268 to 287 pm. The cerium atoms fill distorted hexagonal channels within these networks with one short Ce−Rh contact (310 pm in CeRhSb and 311 pm in $CeRhSbH_{0.2}$). Susceptibility and specific heat measurements on $CeRhSbH_{0.2}$ reveal antiferromagnetic ordering at $T_N = 3.6(2)$ K. The experimental magnetic moment in the paramagnetic region is 2.68(5) μ_B/Ce atom. Magnetization measurements below T_N reveal a spin-flip transition in the range 1.6−2.4 T. Resistivity data show metallic behavior and the characteristics of a Kondo system. Thermoelectric power measurements show a distinct maximum around 106 K with a value of 24 μV/K. ^{121}Sb Mössbauer spectroscopic data for CeRhSb and $CeRhSbH_{0.2}$ at 78 K show only one antimony site. The isomer shift is slightly smaller for the hydrogenated sample indicating a slightly higher electron density at the antimony nuclei of $CeRhSbH_{0.2}$.

Introduction

The equiatomic ternary intermetallic compounds containing cerium CeTX (T = transition metal; X = element of the third, fourth, or fifth main group) have intensively been investigated in the last 20 years with respect to their unusual physical properties like valence fluctuations, heavy-fermion behavior, magnetic ordering with anomalously high-ordering temperatures, Kondo semimetals or semiconductors, non-Fermi liquid behavior, or quantum phase transitions.[1−4] These phenomena are believed to arise due to hybridization between the 4f(Ce) electrons and the conduction electrons.

A highly interesting compound within this large CeTX family is the valence-fluctuating ternary antimonide CeRhSb.[5−23] So far more than 80 entries occur for CeRhSb in the current SciFinder Scholar version.[24] CeRhSb is a so-called Kondo semiconductor and exhibits opening at low temperatures of a small pseudogap in the electronic density of states. The orthorhombic TiNiSi type structure of CeRhSb has so far only been investigated on the basis of X-ray powder data.[15] There are several possibilities to influence the physical properties of such a valence-fluctuating compound.

* Authors to whom correspondence should be addressed. E-mail: chevalie@icmcb-bordeaux.cnrs.fr (B.C.); pottgen@uni-muenster.de (R.P.); a.simon@fkf.mpg.de (A.S.).

† Université Bordeaux 1.

‡ Universität Münster.

§ Max-Planck-Institut für Festkörperforschung.

(1) Fujita, T.; Suzuki, T.; Nishigori, S.; Takabatake, T.; Fujii, H.; Sakurai, J. *J. Magn. Magn. Mater.* **1992**, *108*, 35.

(2) Szytuła, A.; Leciejewicz, J. *Handbook of Crystal Structures and Magnetic Properties of Rare Earth Intermetallics*; CRC Press: Boca Raton, FL, 1994.

(3) Kraft, R.; Pöttgen, R.; Kaczorowski, D. *Chem. Mater.* **2003**, *15*, 2998.

(4) Gaudin, E.; Chevalier, B.; Heying, B.; Rodewald, U. Ch.; Pöttgen, R. *Chem. Mater.* **2005**, *17*, 2693.

(5) Malik, S. K.; Adroja, D. T. *Phys. Rev. B* **1991**, *43*, 6277.

(6) Adroja, D. T.; Rainford, B. D. *J. Magn. Magn. Mater.* **1994**, *135*, 333.

(7) Takabatake, T.; Yoshino, T.; Tanaka, H.; Bando, Y.; Fujii, H.; Fujita, T.; Shida, H.; Suzuki, T. *Physica B* **1995**, 206−207, *804*.

(8) Hammond, T. J.; Gehring, G. A.; Suvasini, M. B.; Temmerman, W. M. *Physica B* **1995**, 206−207, *819*.

(9) Hiraoka, T.; Kinoshita, E.; Tanaka, H.; Takabatake, T.; Fujii, H. *J. Magn. Magn. Mater.* **1996**, *153*, 124.

(10) Malik, S. K.; Menon, L.; Pecharsky, V. K.; Gschneidner, K. A., Jr. *Phys. Rev. B* **1997**, *55*, 11471.

(11) Menon, L.; Kayzel, F. E.; de Visser, A.; Malik, S. K. *Phys. Rev. B* **1998**, *58*, 85.

(12) Adroja, D. T.; Rainford, B. D.; Malik, S. K.; Takeya, H.; Gschneidner, K. A., Jr.; Pecharsky, V. K. *J. Alloys Compd.* **1999**, *288*, 7.

(13) Menon, L.; Adroja, D. T.; Rainford, B. D.; Malik, S. K.; Yelon, W. B. *Solid State Commun.* **1999**, *112*, 85.

(14) Yoshino, T.; Echizen, Y.; Takabatake, T.; Sera, M. *Physica B* **2000**, 281−282, *291*.

(15) Salamakha, P.; Sologub, O.; Suemitsu, T.; Takabatake, T. *J. Alloys Compd.* **2000**, *313*, L5.

(16) Kumigashira, H.; Takahashi, T.; Yoshii, S.; Kasaya, M. *Phys. Rev. Lett.* **2001**, *87*, 067206.

10.1021/cm062168a CCC: $37.00
Published on Web 12/07/2006

Substitution of rhodium by palladium in the solid solution $Ce(Rh_{1-x}Pd_x)Sb$ induces the following: (i) in the composition range $0 \le x \le 0.2$ where the system is insulating, a decrease of the gap energy with increasing Pd substitution; (ii) the occurrence of an antiferromagnetic ordering in the range $0.3 \le x \le 0.4$ with T_N's of the order of 3 K.[6,11,25,26] In this substitution, the number of electrons/formula unit increases by one from CeRhSb to CePdSb. Also, for the orthorhombic samples ($0 \le x \le 0.4$), with increasing Pd content, there is a small increase in unit-cell volume (the metallic radius of palladium $r_{Pd} = 137.6$ pm is slightly larger than that of rhodium $r_{Rh} = 134.5$ pm), which may lead to corresponding decrease in the hybridization strength between the conduction electrons and the 4f(Ce) electrons.[11] Another interesting substitution concerns the solid solution $CeRh(Sb_{1-x}Sn_x)$ for $0 \le x \le 0.2$.[21,22,27,28] With increasing tin content an original sequence of the states is observed: Kondo insulator → heavy Fermion metal → non-Fermi liquid which reflects the decrease of the number of electrons by one/formula unit when passing from CeRhSb to CeRhSn. In this case, the unit-cell volume decreases with increasing x.[21] These results indicate that the magnetic ground state of the ternary antimonide CeRhSb is strongly dependent on the steric effect.

Another possibility for strongly influencing the physical behavior of CeTX intermetallics is a hydrogenation reaction.[29−32] To give an example, hydrogen insertion leads to an interesting transition from an intermediate valence state (CeNiIn) to a ferromagnetic behavior ($CeNiInH_{1.8}$)[33] or an increase of the Néel temperature (1.65 K → 3.0 K) in the sequence CePdIn (Kondo antiferromagnet) → $CePdInH_{1.0}$.[34] All results can be interpreted by considering that the hydrogenation of the compounds based on cerium increases the unit cell volume leading to a reduction in the coupling constant J_{cf} between 4f(Ce) and conduction electrons. J_{cf} governs the competition between the indirect magnetic RKKY temperature T_{RKKY} proportional to J_{cf}^2 and the Kondo temperature T_K which exhibits an exponential dependence on J_{cf}. This competition is qualitatively described by the Doniach phase diagram showing that the reduction of J_{cf} favors for CeTX compounds strongly influenced by the Kondo effect the occurrence or the increase of magnetic ordering for cerium.[34] In other words, the hydrogenation can be considered as an application of "negative" pressure on intermetallics, strongly influencing the band structure.

So far, only CeTX intermetallics with an X element of the third or fourth main group have been studied with respect to their hydrogen sorption behavior. We have now extended our investigations with respect to the group V elements. Herein we report on the hydrogen sorption behavior of intermediate valent CeRhSb which transforms to the 3.6(2) K antiferromagnet $CeRhSbH_{0.2}$. Besides the crystal structures and the changes in the magnetic, electric, and thermal properties we have also studied the ^{121}Sb Mössbauer spectra of CeRhSb and $CeRhSbH_{0.2}$ at 78 and 4.2 K.

Experimental Section

Syntheses. Starting materials for the synthesis of CeRhSb were cerium ingots (Johnson Matthey), rhodium powder (Degussa-Hüls, ca. 200 mesh), and antimony lumps (Johnson Matthey), all with stated purities better than 99.9%. Pieces of the cerium ingot were first arc-melted under argon (ca. 600 mbar)[35] to small buttons (ca. 500 mg). The argon was purified before over titanium sponge (870 K), silica gel, and molecular sieves. The cerium button, a cold-pressed pellet (i.d. 6 mm) of the rhodium powder, and pieces of the antimony lump were then weighed in the ideal 1:1:1 atomic ratio and arc-melted under 600 mbar of argon. The product button was remelted three times to ensure homogeneity. The weight loss after the different melting procedures was always smaller than 0.5 wt % (most likely antimony). CeRhSb is stable in air in the form of a compact button and also as a fine-grained powder. Polycrystalline pieces and small single crystals exhibit metallic luster; powders are dark gray.

Hydrogen absorption experiments were performed using the apparatus described previously.[36] An annealed ingot of CeRhSb was heated under vacuum at 523 K for 12 h and then exposed to 4 MPa of hydrogen gas at the same temperature for 4 days. These conditions are similar to those used previously for the hydrogenation of CePdIn, CePdSn,[34] and many CeNiX compounds.[30] The hydrogenation induces a decrepitation of the starting ingot. The amount of hydrogen absorbed was determined volumetrically by monitoring pressure changes in a calibrated volume. Under these conditions, the new hydride $CeRhSbH_{0.20(5)}$ was obtained. The latter is stable in ambient conditions. We note also that CeRhSb absorbs less hydrogen than CeNiSn[30] or CePdSn[34] which crystallize as the ternary antimonide in the orthorhombic TiNiSi-type structure. Perhaps the presence of Sb induces a decrease of the hydrogen solubility. More experiments at higher pressures and temperatures are necessary to solve this behavior.

EDX Analyses. The single crystal measured on the diffractometer and the bulk sample were analyzed by energy dispersive analyses of X-rays using a Leica 420i scanning electron microscope and CeO_2, Rh, and Sb as standards. The crystal mounted on a quartz fiber was first coated with a thin carbon film to ensure conductivity. The polycrystalline sample was embedded in a metacrylate matrix

(17) Okamura, H.; Matsunami, M.; Nanba, T.; Suemitsu, T.; Yoshino, T.; Takabatake, T.; Isikawa, Y.; Harima, H. *Physica B* **2002**, 312−313, *218*.
(18) Haase, M. G.; Schmidt, T.; Richter, C. G.; Block, H.; Jeitschko, W. *J. Solid State Chem.* **2002**, *168*, 18.
(19) Kitagawa, J.; Sasakawa, T.; Suemitsu, T.; Echizen, Y.; Takabatake, T. *Phys. Rev. B* **2002**, *66*, 224304.
(20) Takabatake, T.; Sasakawa, T.; Kitagawa, J.; Suemitsu, T.; Echizen, Y.; Umeo, K.; Sera, M.; Bando, Y. *Physica B* **2003**, *328*, 53.
(21) Ślebarski, A.; Zawada, T.; Spałek, J.; Jezierski, A. *Phys. Rev. B* **2004**, *70*, 235112,
(22) Spałek, J.; Ślebarski, A.; Goraus, J.; Spałek, L.; Tomala, K.; Zarzycki, A.; Hackemer, A. *Phys. Rev. B* **2005**, *72*, 155112.
(23) Ślebarski, A. *J. Alloys Compd.* **2006**, in press.
(24) 81 entries occur for the formula CeRhSb in the SciFinder Scholar version 2006: http://www.cas.org/SCIFINDER/SCHOLAR/.
(25) Menon, L.; Malik, S. K. *Solid State Commun.* **1997**, *101*, 779.
(26) Menon, L.; Malik, S. K. *Phys. Rev. B* **1997**, *55*, 14100.
(27) Ślebarski, A.; Zawada, T.; Spałek, J. *Physica B* **2005**, *359−361*, 118.
(28) Ślebarski, A.; Spałek, J. *Phys. Rev. Lett.* **2005**, *95*, 046402.
(29) Chevalier, B.; Bobet, J.-L.; Pasturel, M.; Gaudin, E.; Etourneau, J. *J. Alloys Compd.* **2003**, *356−357*, 147.
(30) Chevalier, B.; Pasturel, M.; Bobet, J.-L.; Decourt, R.; Etourneau, J.; Isnard, O.; Sanchez Marcos, J.; Rodriguez Fernandez, J. *J. Alloys Compd.* **2004**, *383*, 4.
(31) Chevalier, B.; Pasturel, M.; Bobet, J.-L.; Isnard, O. *Solid State Commun.* **2005**, *134*, 529.
(32) Bobet, J.-L.; Pasturel, M.; Chevalier, B. *Intermetallics* **2006**, *14*, 544.
(33) Chevalier, B.; Kahn, M. L.; Bobet, J.-L.; Pasturel, M.; Etourneau, J. *J. Phys.: Condens. Matter* **2002**, *14*, L365.
(34) Chevalier, B.; Wattiaux, A.; Bobet, J.-L. *J. Phys.: Condens. Matter* **2006**, *18*, 1743.
(35) Pöttgen, R.; Gulden, Th.; Simon, A. *GIT Labor-Fachz.* **1999**, *43*, 133.
(36) Bobet, J.-L.; Pechev, S.; Chevalier, B.; Darriet, B. *J. Alloys Compd.* **1998**, *267*, 136.

Table 1. Crystal Data and Structure Refinement for CeRhSb and $CeRhSbH_{0.2}$ with TiNiSi Type Structure (*Pnma*, $Z = 4$)

empirical formula	CeRhSb	$CeRhSbH_{0.2}$
molar mass (g/mol)	364.78	364.98
unit cell dimens (Guinier powder data) (pm)	$a = 741.58(9)$	$a = 742.2(2)$
	$b = 461.80(9)$	$b = 462.5(2)$
	$c = 785.77(8)$	$c = 787.7(2)$
V (nm^3)	0.2691	0.2704
calcd density (g/cm^3)	9.00	8.96
cryst size (μm^3)	$20 \times 20 \times 20$	$15 \times 30 \times 40$
transm ratio (max/min)	2.07	1.94
abs coeff (mm^{-1})	32.3	32.1
$F(000)$	616	616
θ range (deg)	3−35	3−30
range in *hkl*	±11, ±7, ±12	±10, ±6, ±11
tot. no. reflections	4317	2645
independent reflections	645 ($R_{int} = 0.0710$)	443 ($R_{int} = 0.0628$)
reflections with $I > 2\sigma(I)$	491 ($R_\sigma = 0.0373$)	331 ($R_\sigma = 0.0425$)
data/params	645/20	443/20
goodness-of-fit on F^2	1.193	1.224
final R indices [$I > 2\sigma(I)$]	R1 = 0.0434	R1 = 0.0561
	wR2 = 0.0873	wR2 = 0.1409
R indices (all data)	R1 = 0.0661	R1 = 0.0723
	wR2 = 0.0960	wR2 = 0.1444
extinction coeff	0.0009(4)	0.0016(6)
largest diff peak and hole ($e/Å^3$)	3.19/−4.52	8.23/−3.54

and polished with different diamond and SiO_2 emulsions. The analyses (33 ± 3 at. % Ce; 36 ± 3 at. % Rh; 31 ± 3 at. % Sb) were in good agreement with the ideal composition. The larger standard uncertainty accounts for the measurements at different points. No impurity elements have been detected. The hydrogenated sample shows similar results.

X-ray Powder Diffraction. The samples (precursors and the hydrided samples) were routinely characterized by X-ray powder diffraction either by the Guinier technique (Cu $K\alpha_1$ radiation, α-quartz: $a = 491.30$ and $c = 540.46$ pm as internal standard) or on a Stoe StadiP powder diffractometer (Cu $K\alpha_1$ radiation, silicon: $a = 543.07$ pm as an external standard). The Guinier camera was equipped with an imaging plate technique (Fujifilm, BAS-READER 1800). The orthorhombic lattice parameters given in Table 1 were obtained from least-squares fits to the X-ray powder data. To ensure correct indexing, the experimental patterns were compared with calculated ones,[37] taking the atomic positions from the structure refinements. The lattice parameters reported here for CeRhSb are in very good agreement with the available literature data.[15,18]

Single-Crystal X-ray Data. Irregularly shaped single crystals were isolated by mechanical fragmentation from the arc-melted precursor sample as well as from the hydrogenated sample. These crystals were first investigated on a Buerger precession camera (white Mo radiation, Fujifilm imaging plate) to check the quality for intensity data collection. The crystals of $CeRhSbH_{0.2}$ were taken directly from the crumbled sample after the hydrogenation process. More than 100 crystallites were checked, but only medium-quality crystals of $CeRhSbH_{0.2}$ were found.

Data sets of a CeRhSb and a $CeRhSbH_{0.2}$ crystal were then collected at room temperature on a Stoe IPDS-II diffractometer (Mo Kα radiation) in oscillation mode. Numerical absorption corrections were applied to both data sets. Details on the crystallographic data are given in Table 1.

Hydrogen Analyses. The hydrogen content of the $CeRhSbH_x$ sample was carefully checked by combustion analyses. The sample was burnt in an oxygen atmosphere and the resulting water potentiometrically titrated using an automated Karl Fischer method.[38] The analyses were repeated for three batches (ca. 100 mg each) of the sample. Within the accuracy of the method used (±3%), a hydrogen content of $CeRhSbH_{0.15}$ was detected, in good agreement with the volumetric data.

Magnetization, Electrical Resistivity, Thermoelectric Power, and Specific Heat Measurements. Magnetization measurements were performed on powder samples of CeRhSb and $CeRhSbH_{0.2}$ using a superconducting quantum interference device (SQUID) magnetometer in the temperature range 1.8−300 K and applied fields up to 5 T.

For transport and specific heat measurements, the hydride $CeRhSbH_{0.2}$ was compacted at room temperature (compactness ≅ 80% to form a polycrystalline pellet (diameter = 6 mm and thickness = 3 mm) and then heated for 2 days at 523 K under 4 MPa hydrogen pressure. Thermoelectric power measurements were performed on this pellet using a dynamic method. Details of the cell used and the measurement methods have been described previously.[39] For electrical resistivity, a bar of $1.5 \times 1.5 \times 5$ mm^3 was cut from the pellet. The measurement was carried out above 4.2 K using a standard dc four probe method with silver paint contacts and an intensity current of 10 mA. Heat capacity measurement was realized on a plate obtained from the pellet, by a relaxation method with a Quantum Design PPMS system and using a two τ model analysis.

^{121}Sb Mössbauer Spectroscopy. A $Ba^{121m}SnO_3$ source was used for the Mössbauer spectroscopic experiments. The measurements were carried out in a helium bath cryostat at 4.2 and 78 K. The temperature was controlled by a resistance thermometer (±0.5 K accuracy). The Mössbauer source was kept at room temperature. The samples were enclosed in small PVC containers at a thickness corresponding to about 10 mg of Sb/cm^2.

Results and Discussion

Structure Refinements. The Guinier powder pattern of $CeRhSbH_{0.2}$ already revealed isotypy with CeRhSb. The atomic positions of a previous Rietveld refinement on powder[15] were then taken as starting values, and both structures were refined using SHELXL-97 (full-matrix least squares on F^2)[40] with anisotropic atomic displacement parameters for all atoms. Due to the small hydrogen content, the low crystal quality, and the very weak scattering power of the hydrogen atoms, hydrogen sites of $CeRhSbH_{0.2}$ could definitely not be determined. The occupancy parameters were refined in separate series of least-squares cycles. All sites were fully occupied within two standard uncertainties, and the ideal composition was assumed again in the final cycles. A final difference electron-density synthesis was flat for CeRhSb and did not reveal any significant residual peaks. Due to the low crystal quality of the hydride, higher residual peaks remained for $CeRhSbH_{0.2}$. The results of the structure refinements are summarized in Table 1. The atomic coordinates and the interatomic distances are listed in Tables 2 and 3. Further information on the structure refinements are available. (Details may be obtained from Fachinformationszentrum Karlsruhe, D-76344 Eggenstein-Leopoldshafen, Germany, by quoting the Registry No's. CSD-416610 (CeRhSb) and CSD-416611 ($CeRhSbH_{0.2}$).)

(37) Yvon, K.; Jeitschko, W.; Parthé, E. *J. Appl. Crystallogr.* **1977**, *10*, 73.
(38) Eger, R.; Mattausch, Hj.; Simon, A. *Z. Naturforsch.* **1993**, *48b*, 48.
(39) Dordor, P.; Marquestaut, E.; Villeneuve, G. *Rev. Phys. Appl.* **1980**, *15*, 1607.
(40) Sheldrick, G. M. *SHELXL-97, Program for Crystal Structure Refinement*; University of Göttingen: Göttingen, Germany, 1997.

Table 2. Atomic Coordinates and Isotropic Displacement Parameters (pm^2) of CeRhSb and $CeRhSbH_{0.2}$

atom	Wyck	*x*	*y*	*z*	U_{eq}[a]
		CeRhSb			
Ce	4*c*	0.0116(1)	1/4	0.6997(1)	83(2)
Rh	4*c*	0.3027(2)	1/4	0.4166(2)	108(3)
Sb	4*c*	0.1892(1)	1/4	0.0896(1)	73(2)
		$CeRhSbH_{0.2}$			
Ce	4*c*	0.0117(2)	1/4	0.7002(2)	59(5)
Rh	4*c*	0.3032(3)	1/4	0.4171(3)	73(6)
Sb	4*c*	0.1892(3)	1/4	0.0897(3)	44(5)

[a] U_{eq} is defined as one-third of the trace of the orthogonalized $\mathbf{U}_{ij}$ tensor.

Table 3. Interatomic Distances (pm), Calculated with the Powder Lattice Parameters of CeRhSb and $CeRhSbH_{0.2}$[a]

atom 1	atom 2	CeRhSb	$CeRhSbH_{0.2}$
Ce	1 Rh	310.0	310.7
	2 Rh	318.3	318.7
	2 Sb	320.8	321.1
	1 Sb	329.8	330.9
	2 Sb	331.7	332.2
	1 Sb	333.5	333.8
	1 Rh	339.0	338.8
	2 Rh	340.6	341.5
	2 Ce	379.1	379.3
	2 Ce	390.0	391.5
Rh	2 Sb	268.0	268.3
	1 Sb	270.4	271.5
	1 Sb	286.6	286.6
	1 Ce	310.0	310.7
	2 Ce	318.3	318.6
	1 Ce	339.0	338.8
	2 Ce	340.6	341.5
Sb	2 Rh	268.0	268.3
	1 Rh	270.4	271.5
	1 Rh	286.6	286.6
	2 Ce	320.8	321.1
	1 Ce	329.8	330.9
	2 Ce	331.7	332.2
	1 Ce	333.5	333.8

[a] Standard deviations are all equal or less than 0.3 pm. All distances within the first coordination spheres are listed.

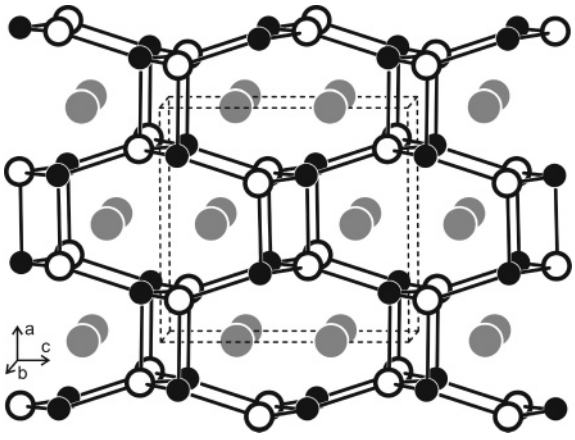

Figure 1. Crystal structure of CeRhSb. Cerium, rhodium, and antimony atoms are drawn as medium gray, black-filled, and open circles, respectively. The three-dimensional [RhSb] network is emphasized.

Crystal Chemistry. The structure of CeRhSb was refined from single-crystal diffractometer data for the first time. Our data confirm the previous Rietveld data,[15] but the atomic positions have been refined with higher precision. A view of the CeRhSb structure approximately along the *b*-axis is presented in Figure 1. The rhodium and antimony atoms build up a three-dimensional [RhSb] network in which the cerium atoms are embedded. Both rhodium and antimony have a strongly distorted tetrahedral coordination with Rh−Sb distances ranging from 268 to 287 pm (Table 3), slightly longer than the sum of the covalent radii of 266 pm.[41] We can thus assume significant Rh−Sb bonding interactions.

The Ce−Rh (310−341 pm) and Ce−Sb (321−334 pm) distances are both longer than the sums of the covalent radii[41] of 290 and 306 pm, respectively. This behavior is different from that of the germanide CeRhGe,[4] where very short Ce−Rh contacts of 295 pm have been observed, and electronic structure calculations revealed that these are the strongest bonding interactions in the latter compound. The Ce−Ce distances cover the range from 379 to 390 pm. They are well above the Hill limit for 4f electron localization.[42] Thus, the Ce−Ce interactions are not the main reason for the intermediate-valent behavior of CeRhSb. The various facets of the crystal chemistry of TiNiSi-related intermetallics has been discussed in detail in a recent work. For further information we refer to this literature.[43−47]

We will now switch to the new hydride $CeRhSbH_{0.2}$, which crystallizes in the same structure as CeRhSb (Tables 1 and 2). This behavior is comparable to that observed during the hydrogenation of the orthorhombic ternary stannides CeNiSn[30, 48−51] and CePdSn;[34] the hydrides $CeNiSnH_{1.0}$ and $CePdSnH_{1.0}$ also adopt the orthorhombic TiNiSi-type structure. In this structure, two types of chemically similar but geometrically different (Ce_3Ni or Ce_3Pd) tetrahedra are formed; only one that has a nearly regular Ce_3 side is fully occupied by a hydrogen atom.[51] The other significantly deformed (Ce_3Ni or Ce_3Pd) tetrahedron is empty.

In going from CeRhSb to $CeRhSbH_{0.2}$, we observe an isotropic increase of the orthorhombic lattice parameters and the increase in cell volume is about 0.5% by hydrogen inserted (Table 1). Such a tiny increase in volume has so far only been observed for hydrogenation of CeNiSi[52] but agrees with those detected during the hydrogenation of CeNiSn[30] and CePdSn,[34] respectively 2.6 and 2.5% by hydrogen inserted. As is evident from Table 3, we observe a small, overall increase of the interatomic distances in $CeRhSbH_{0.2}$. On the basis of the single-crystal X-ray data for $CeRhSbH_{0.2}$, we could clearly confirm the cerium, rhodium, and antimony positions. In view of the low crystal quality and the minor hydrogen content, however, it was definitely not possible to determine any hydrogen sites. As

(41) Emsley, J. *The Elements*; Clarendon Press: Oxford, U.K., 1989.
(42) Hill, H. H. In *Plutonium and Other Actinides*; Mines, W. N., Ed.; Nuclear Materials Series; AIME: New York, 1970; Vol. 17, p 2.
(43) Nuspl, G.; Polborn, K.; Evers, J.; Landrum, G. A.; Hoffmann, R. *Inorg. Chem.* **1996**, *35*, 6922.
(44) Landrum, G. A.; Hoffmann, R.; Evers, J.; Boysen, H. *Inorg. Chem.* **1998**, *37*, 5754.
(45) Hoffmann, R.-D.; Pöttgen, R. *Z. Kristallogr.* **2001**, *216*, 127.
(46) Bojin, M. D.; Hoffmann, R. *Helv. Chim. Acta* **2003**, *86*, 1653.
(47) Bojin, M. D.; Hoffmann, R. *Helv. Chim. Acta* **2003**, *86*, 1683.
(48) Chevalier, B.; Bobet, J.-L.; Pasturel, M.; Bauer, E.; Weill, F.; Decourt, R.; Etourneau, J. *Chem. Mater.* **2003**, *15*, 2181.
(49) Chevalier, B.; Wattiaux, A.; Fournès, L.; Pasturel, M. *Solid State Sci.* **2004**, *6*, 573.
(50) Chevalier, B.; Pasturel, M.; Bobet, J.-L.; Etourneau, J.; Isnard, O.; Sanchez Marcos, J.; Rodriguez Fernandez, J. *J. Magn. Magn. Mater.* **2004**, *576*, 272−276.
(51) Yartys, V. A.; Ouladdiaf, B.; Isnard, O.; Khyzhun, O. Yu.; Buschow, K. H. J. *J. Alloys Compd.* **2003**, *359*, 62.
(52) Pasturel, M.; Bobet, J.-L.; Isnard, O.; Chevalier, B. *J. Alloys Compd.* **2004**, *384*, 39.

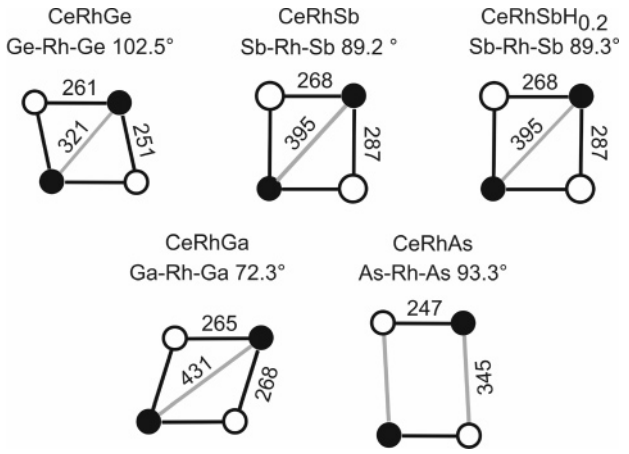

Figure 2. Comparison of the interatomic distances and bond angles in the Rh_2X_2 (X = Ge, Sb, Ga, As) parallelograms in CeRhGe, CeRhSb, $CeRhSbH_{0.2}$, CeRhGa, and CeRhAs. The transition metal and X atoms are drawn as filled and open circles, respectively. The standard deviations for the bond distances and angles are equal or smaller than 0.3 pm and 0.1°. For details, see the text.

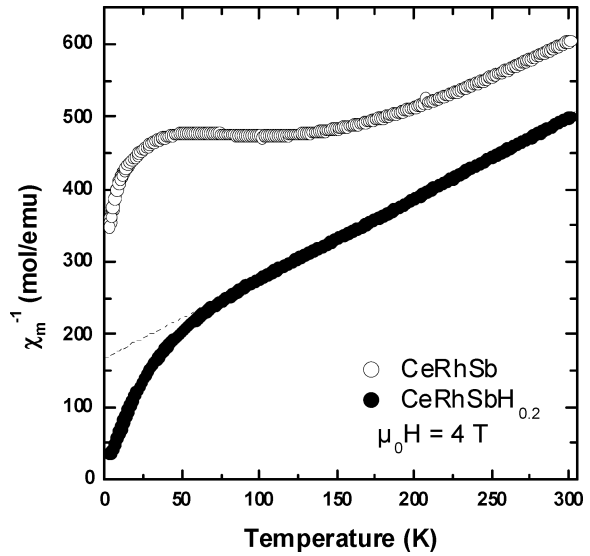

Figure 3. Temperature dependence of the reciprocal magnetic susceptibility, measured with an applied field $\mu_0 H = 4$ T, of CeRhSb and its hydride. The dashed line shows the Curie−Weiss law (see text).

discussed above, the CeRhSb structure leaves various distorted tetrahedral voids where the few hydrogen atoms are most likely accommodated.

Finally we wish to discuss the CeRhSb and $CeRhSbH_{0.2}$ structures in line with other CeRhX compounds which crystallize with a TiNiSi related structure. In Figure 2 we present the Rh_2X_2 (X = Ge, Sb, Ga, As) parallelograms which occur in the polyanionic networks of CeRhGe,[4] CeRhSb, $CeRhSbH_{0.2}$, CeRhGa,[53] and CeRhAs.[15] In each compound we observe one short Rh−X intralayer contact with a distance close to the sum of the covalent radii. For CeRhGe, CeRhSb, $CeRhSbH_{0.2}$, and CeRhGa, also the interlayer Rh−X distances fall in the same range, while a much longer interlayer Rh−As distance of 345 pm occurs for CeRhAs.[15] Thus, we do not observe bonding Rh−As interactions between the layers. This is a unique situation for TiNiSi-related intermetallics, and consequently, the relationship of CeRhAs with the other CeRhX compounds should be called isopointal[54,55] rather than isotypic. This is certainly the structural prerequisite for the interesting high-pressure behavior (phase transitions) of CeRhAs.[56]

Another interesting feature concerns the tilt of the Rh_2X_2 parallelograms. In CeRhSb and $CeRhSbH_{0.2}$ we observe an almost rectangular arrangement, while a left- and right-tilted Rh_2Ge_2 and Rh_2Ga_2 parallelogram occurs in CeRhGe and CeRhGa, respectively. In a recent electronic structure investigation of various TiNiSi-related intermetallic compounds Nuspl et al. have demonstrated[43] that always the more electronegative atoms show the maximum separation within the parallelograms. In this view, the electronic structures of CeRhGe and CeRhGa are significantly different. However, it is not possible to correlate the structural distortion with the magnetic ground state of the respective compound. Both CeRhSb and CeRhAs are intermediate-valent compounds, but the tilt is different. The same holds true for the antiferromagnets $CeRhSbH_{0.2}$ ($T_N = 3.6$ K) and CeRhGe ($T_N = 9.3$ K). Detailed investigations of the electronic structures of these materials are in progress.

Magnetism. Figure 3 presents the temperature dependence of the reciprocal magnetic susceptibility χ_m^{-1} of CeRhSb and its hydride. An appreciable increase in the χ_m value of the hydride is observed relative to that of CeRhSb.

The curve $\chi_m^{-1} = f(T)$ concerning CeRhSb shows a broad minimum around 105−110 K and that the decrease of χ_m^{-1} below 30−40 K might originate from a small amount of free Ce^{3+} ion stabilized lattice defects or a trace of some paramagnetic impurities. This behavior is typical of intermediate valence system containing small quantities of magnetic impurities. These data obtained here on CeRhSb are in agreement with those reported earlier.[5,10,21,25] According to the model proposed by Lawrence et al.,[57] T_K (Kondo temperature) is defined below the broad minimum as $T_K = C/2\chi_m(0)$, where $C = 0.807$ emu K/(Ce mol) is the Curie constant for free Ce^{3+} ions and $\chi_m(0)$ the magnetic susceptibility at $T = 0$ K. This model forecasts that the $\chi_m^{-1} = f(T)$ curve exhibits a broad minimum at $T_{min} = T_K/2$. $\chi_m(0)$ is obtained by fitting of χ_m^{-1} at low temperature according to $\chi_m^{-1} = (\chi_m(0) + nC/T)^{-1}$, where n is the proportion of stable Ce^{3+} (impurities). For CeRhSb, the following values are obtained: $n = 3.23 \times 10^{-3}$ Ce^{3+}/mol; $\chi_m(0) = 2.06 \times 10^{-3}$ emu/(Ce mol); $T_K = 198(5)$ K. Half of this Kondo temperature ($T_K/2 = 99$ K) is comparable to the location of the broad minimum one ($T_{min} = 105-110$ K). On the contrary, above 110 K, the data relative to the hydride $CeRhSbH_{0.2}$ can be fitted with a Curie−Weiss law giving $\Theta_p = -151(3)$ K and $\mu_{eff} = 2.68(5)$ μ_B/mol. The effective moment value is close to that calculated for a free Ce^{3+} ion (2.54 μ_B). The negative curvature observed at low temperatures in the $\chi_m^{-1} = f(T)$ curve indicates the presence of a crystal-field effect. In other words, hydrogenation of the ternary antimonide CeRhSb induces a change of the valence state of cerium from

(53) Chevalier, B.; Heying, B.; Pöttgen, R. Unpublished results.
(54) Gelato, L. M.; Parthé, E. *J. Appl. Crystallogr.* **1987**, *20*, 139.
(55) Parthé, E.; Gelato, L. M. *Acta Crystallogr.* **1984**, *40A*, 169.
(56) Uemo, K.; Masumori, K.; Sasakawa, T.; Iga, F.; Takabatake, T.; Ohishi, Y.; Adachi, T. *Phys. Rev. B* **2005**, *71*, 064110.
(57) Lawrence, J. M.; Riseborough, P. S.; Parks, R. D. *Rep. Prog. Phys.* **1981**, *44*, 1.

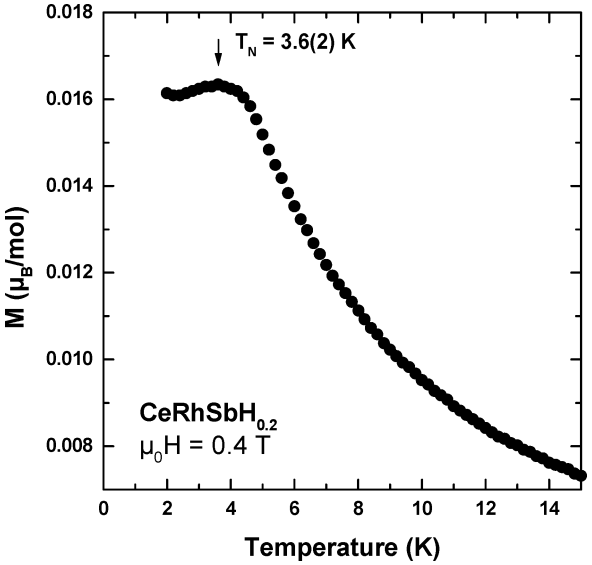

Figure 4. Temperature dependence of the magnetization, measured with an applied field $\mu_0 H = 0.4$ T, of $CeRhSbH_{0.2}$.

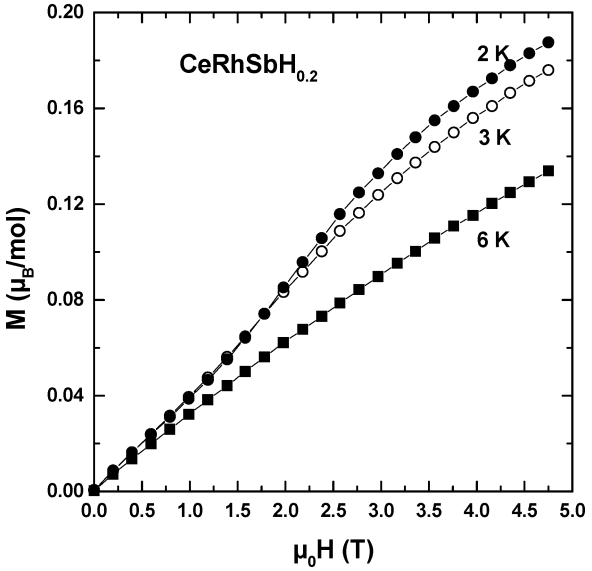

Figure 5. Field dependence of the magnetization of $CeRhSbH_{0.2}$ measured above T_N (6 K) and below T_N (3 and 2 K).

intermediate to purely trivalent. Similar behavior was observed previously by hydrogenation of the Kondo semiconductor CeNiSn.[30,50,51] The hydride $CeNiSnH_{1.0}$ which crystallizes as CeNiSn or CeRhSb in the orthorhombic TiNiSi-structure type contains trivalent cerium and orders antiferromagnetically below $T_N = 4.5(2)$ K.

The presence of a broad maximum at $T_N = 3.6(2)$ K in the temperature dependence of the magnetization of the hydride $CeRhSbH_{0.2}$ (Figure 4) suggests an antiferromagnetic ordering of the Ce magnetic moments. This magnetic ordering is further corroborated by the field-dependent behavior of the magnetization taken below T_N (Figure 5). At 2 and 3 K and up to $\mu_0 H \leq 4.8$ T, in the antiferromagnetic range, the magnetization of $CeRhSbH_{0.2}$ increases linearly at low fields, more rapidly in the range 1.6−2.4 T, and then exhibits a curvature. This behavior suggests the occurrence of a magnetic transition induced by the applied magnetic field as observed in many antiferromagnets (spin-flip or spin-flop transition). At 2 K and $\mu_0 H = 4.8$ T the value of the

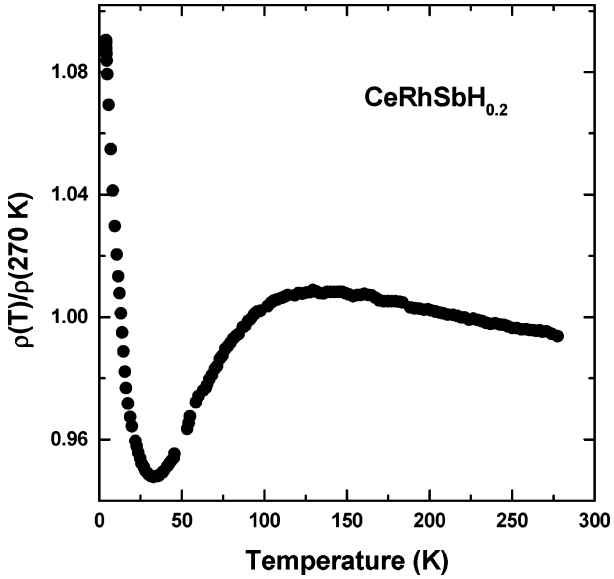

Figure 6. Temperature dependence of the reduced electrical resistivity for the hydride $CeRhSbH_{0.2}$.

magnetization ≅0.19(1) μ_B/Ce is clearly smaller than that calculated for a free Ce^{3+} ion (2.14 μ_B) may be due to the (i) crystal-field and/or (ii) Kondo effects which can reduce the Ce-magnetic moment. Detailed ac susceptibility measurements are planned to analyze the nature of magnetic ordering in $CeRhSbH_{0.2}$ (the broad transition and the partial hydrogen occupancy might induce spin glass behavior) more deeply.

Finally, it should be mentioned that the Néel temperature of the hydride $CeRhSbH_{0.2}$ is comparable to that reported for the compounds $Ce(Rh_{1-x}Pd_x)Sb$ with $0.3 \leq x \leq 0.4$ which order antiferromagnetically around 3 K.[25,26] The Pd substitution or the hydrogenation of CeRhSb lead to an expansion of the unit cell volume which favors a decrease of the hybridization between the 4f(Ce) and the conduction electrons. The magnetic Ruderman−Kittel−Kasuya−Yosida (RKKY) interaction, which drives the compound toward a long-range magnetic ordering, increases whereas the Kondo interaction, which tends to demagnetize the 4f(Ce) states, decreases.[30,33,34]

Resistivity. The temperature dependence of the reduced electrical resistivity of $CeRhSbH_{0.2}$, measured above 4.2 K, exhibits some characteristics of Kondo systems and presents some similarities with that of CeRhSb (Figure 6).[5,7,9,10] (Due to the presence of porosities and microcracks resulting from the low temperature (523 K) used during the annealed treatment performed on this sample, the absolute value of $\rho(T)$ could not be determined accurately; for this reason, the reduced resistivity is reported.) The curve $\rho(T)/\rho(270\text{ K}) = f(T)$ for $CeRhSbH_{0.2}$ reveals several anomalies: (i) A broad maximum occurs around 129 K. (ii) Below this maximum, $\rho(T)$ decreases and a minimum appears near 33 K. (iii) Finally, below this minimum there is a rise of $\rho(T)$ down to 4.2 K. In the two temperature ranges 130−270 K and 7−17 K, the law $\rho(T)/\rho(270\text{ K}) = -A \log T$ (A = constant) is observed. Such behaviors are expected for Kondo-type interactions in the presence of crystal-field effects.[58] The high-temperature logarithmic regime represents the Kondo

(58) Cornut, B.; Coqblin, B. *Phys. Rev. B* **1972**, *5*, 4541.

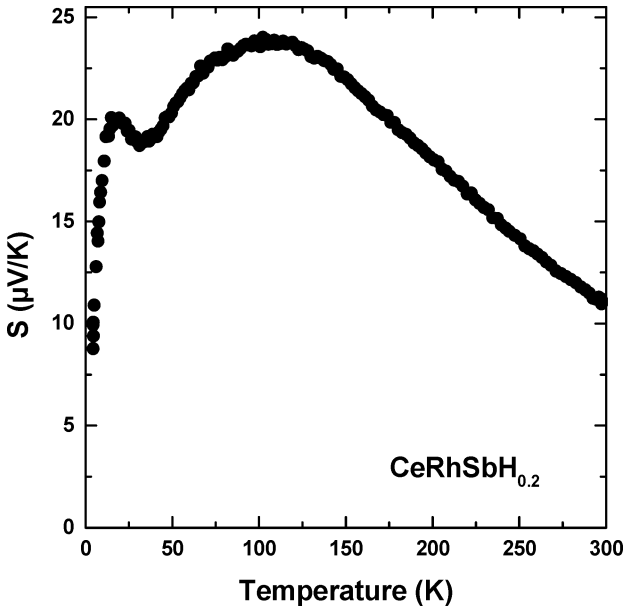

Figure 7. Temperature dependence of the thermoelectric power for the hydride $CeRhSbH_{0.2}$.

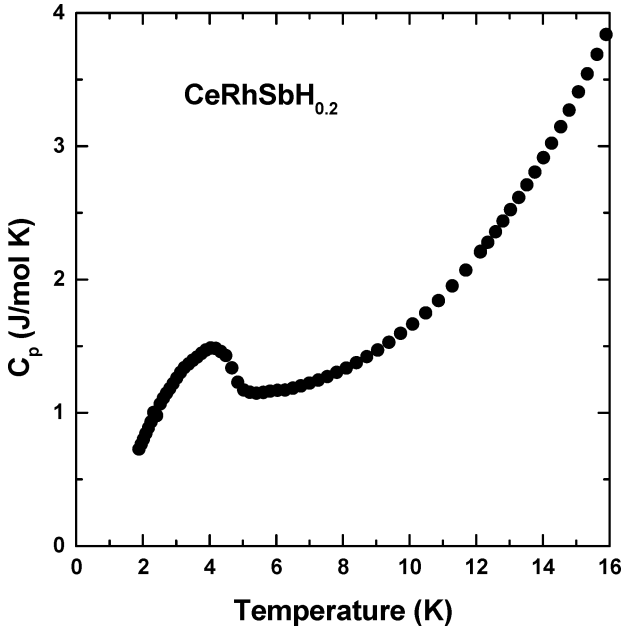

Figure 8. Temperature dependence of the specific heat C_p in the hydride $CeRhSbH_{0.2}$.

effect in the excited doublet (we note that the temperature 120−130 K where the $\rho(T)/\rho(270\ \mathrm{K}) = \mathrm{f}(T)$ curve shows a maximum is practically in agreement with 110 K where the magnetic susceptibility exhibits a negative deviation from the Curie−Weiss law (Figure 3)), whereas the low-temperature regime is related to the Kondo effect from the crystal-field ground state. As the measurements were performed above 4.2 K (i.e., higher than the Néel temperature T_N = 3.6(2) K), no decrease is evidenced at lower temperature. The comparison of the $\rho(T)$ curves between CeRhSb and its hydride indicates that (i) the temperatures where the broad maximum occurs are comparable, 129 K and 113 or 150 K respectively for $CeRhSbH_{0.2}$ (this work) and CeRhSb[5,10] and (ii) the rapid increase observed at low temperature is less pronounced for the hydride $CeRhSbH_{0.2}$. For instance the ratio $\rho(4.2\ \mathrm{K})/\rho(T_{min})$ (T_{min} = 33 K, the temperature of the minimum) is close to 1.15 for $CeRhSbH_{0.2}$ whereas it takes the value 1.67 or 3.0 for CeRhSb.[5,9] This last result indicates the gap formation in the electronic density of states as observed for the parent antimonide CeRhSb,[5,9,10] but the gap energy decreases in the sequence CeRhSb → $CeRhSbH_{0.2}$.

Thermopower. Figure 7 shows the temperature dependence of the thermoelectric power S of $CeRhSbH_{0.2}$. Knowing that the S-values can be influenced by the small density (≅80%) of the compacted hydride sample, we have performed thermoelectric power measurements on a pellet of CeRhSb obtained by pressing at room temperature and then heated 2 days at 523 K under 4 MPa purified argon pressure. The S-values measured here agree with those reported previously;[59] the absolute values of S differ only of 5%. The curve $S = \mathrm{f}(T)$ of the hydride exhibits many similarities to that reported for the initial antimonide CeRhSb investigated both on the polycrystalline sample[20,59] or single crystal.[7] It is mainly characterized by the existence of two positive maxima: one of about 24 μV/K near 106 K and the second more narrow at 20 μV/K around 17 K followed by a rapid decrease. Between them, the thermoelectric power passes through a broad minimum close to 30 K. The broad positive peak at higher temperature (106 K) is ascribed to an interplay of the Kondo and the crystalline electric field (CEF) effects.[60] The peak value measures the strength of the Kondo effect, and the peak temperature determines the CEF splitting. The temperature ≅106 K of this broad maximum is comparable to those where the curve $\rho(T)/\rho(270\ \mathrm{K}) = \mathrm{f}(T)$ (Figure 6) shows also a maximum and the curve $\chi_m^{-1} = \mathrm{f}(T)$ (Figure 3) deviates from the Curie−Weiss law. These three measurements are in agreement for the determination of the CEF splitting existing in the hydride $CeRhSbH_{0.2}$. It is interesting to note that the value of $S \cong 24\ \mu$V/K of the broad positive peak in hydride is lower than that determined previously on CeRhSb (≅50 μV/K),[20] suggesting a diminution of the strength of the Kondo effect during the hydrogenation. The existence of the narrow peak at lower temperature was explained for CeRhSb as the result of the gapping in the density of states.[7,20,59] Opening of the pseudogap in the hydride $CeRhSbH_{0.2}$ seems to appear in agreement with the occurrence of a similar peak at 17 K, but (i) its S-value ≅ 20 μV/K is smaller than that observed for CeRhSb (≅70 μV/K)[7,20,59] and (ii) on the contrary to the initial antimonide the S-value of the narrow peak at 17 K is smaller than that measured for the broad maximum existing at higher temperature. This result agrees with the electrical resistivity measurement and suggests a decrease of the gap energy after hydrogenation.

Heat Capacity. As presented in Figure 8, the temperature dependence of the specific heat C_p for $CeRhSbH_{0.2}$ exhibits a peak at about 4.1(2) K and a peak value approaching 1.5 J mol^{-1} K^{-1}. The temperature of the heat-capacity peak is practically the same as the temperature of the

(59) Sasakawa, T.; Shigetoh, K.; Hirata, D.; Umeo, K.; Takabatake, T. *Physica B* **2005**, *359*−361, 111.

(60) Zlatic, V.; Horvatic, B.; Milat, I.; Coqblin, B.; Czycholl, G.; Grenzebach, C. *Phys. Rev. B* **2003**, *68*, 104432.

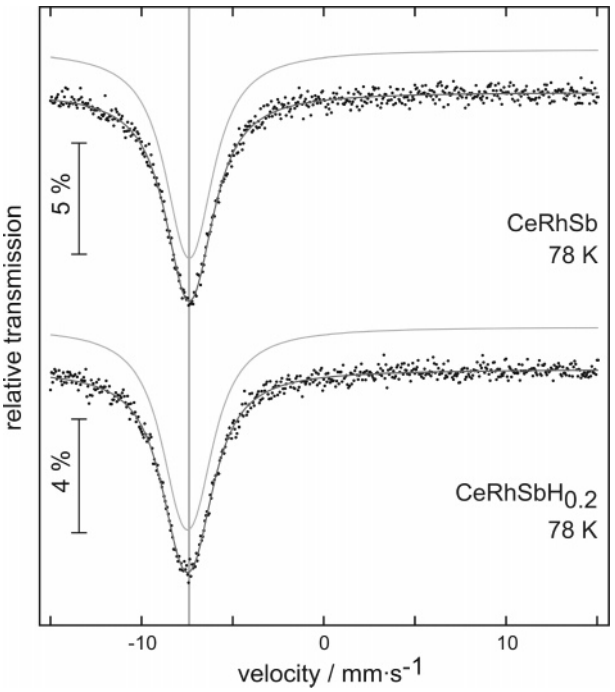

Figure 9. Experimental and simulated ^{121}Sb Mössbauer spectra of CeRhSb and $CeRhSbH_{0.2}$ at 78 K.

susceptibility maximum (Figure 4). The occurrence of this anomaly on the $C_p = f(T)$ curve of the hydride $CeRhSbH_{0.2}$ characterizes its antiferromagnetic ordering. This behavior, not observed in the specific heat measurement performed on CeRhSb,[10,59,61,62] shows some similarities with those reported for $Ce(Rh_{0.7}Pd_{0.3})Sb$,[11] which orders antiferromagnetically around 3 K. Valuable information can be obtained from the entropy associated with the antiferromagnetic ordering of $CeRhSbH_{0.2}$, which is estimated from the magnetic contribution to the specific heat in the low-temperature range ($T \leq 16$ K) as $C_{p\,\mathrm{mag}} = C_p - (\gamma T + \beta T^3)$ (the LaRhSb specific heat[62] has been taken as the phonon contribution C_{ph} for $CeRhSbH_{0.2}$ with an electronic coefficient $\gamma = 8.2$ mJ mol^{-1} K^{-2} and phonon constant $\beta = 0.29$ mJ mol^{-1} K^{-4}). At T_N, the magnetic entropy reaches 1.25 J mol^{-1} K^{-1} $= 0.22R$ ln 2, which is substantially reduced from R ln 2 $= 5.76$ J mol^{-1} K^{-1}, the value of magnetic entropy expected for a doublet ground state of Ce^{3+}. This reduction suggests the presence of a significant Kondo effect in the hydride $CeRhSbH_{0.2}$. This agrees with the strong electronic term $\gamma = 290(20)$ mJ mol^{-1} K^{-2} deduced from the fitting of the experimental data for $T \leq 3.1$ K. This γ value appears remarkably enhanced, as is observed in magnetically ordered heavy-fermion systems like $Ce(Ru_{0.4}Rh_{0.6})_2Si_2$ ($\gamma = 300$ mJ mol^{-1} K^{-2}).[63,64] Moreover, the γ value for $CeRhSbH_{0.2}$ is higher than that extrapolated to 0 K (30 mJ mol^{-1} K^{-2})[10] for the ternary antimonide CeRhSb in agreement with the decrease of the pseudogap induced by the hydrogenation.

^{121}Sb Mössbauer Spectroscopy. ^{121}Sb Mössbauer spectra of CeRhSb and $CeRhSbH_{0.2}$ taken at 78 K are presented in Figure 9 together with transmission integral fits. Both spectra show single signals, in agreement with the single antimony sites observed from the structure refinements. Due to the noncubic site symmetry, the spectra are subject to weak quadrupole splitting. The following fitting parameters (isomer shift δ, line width Γ, electric quadrupole splitting ΔE_Q) have been obtained: $\delta = -7.38(1)$, $\Gamma = 2.90(6)$, $\Delta E_Q = 0.67(10)$ mm/s for CeRhSb; $\delta = -7.47(1)$, $\Gamma = 2.87(7)$, $\Delta E_Q = 0.85(8)$ mm/s for $CeRhSbH_{0.2}$. The 4.2 K spectra (not shown) show almost identical data. No transferred hyperfine field could be detected in the 4.2 K spectrum of the 3.6 K antiferromagnet $CeRhSbH_{0.2}$.

The isomer shifts of both samples compare well with the data obtained for the equiatomic YbTSb (T = Ni, Cu, Pd, Ag, Pt, Au) antimonides[65] as well as the related materials AlSb, GaSb, InSb, CdSb, or SnSb.[66] The isomer shifts of the various ionic and covalent antimony compounds have been summarized and evaluated by Lippens.[66] He correlated the isomer shift with the calculated values of the electron density at the antimony nuclei. This linear correlation clearly revealed an increase of the electron density with decreasing isomer shift. Consequently, we observe a slightly higher electron density at the antimony nuclei in $CeRhSbH_{0.2}$. This behavior is similar to that for the stannides/hydrides CeRhSn/$CeRhSnH_{0.8}$ and CeIrSn/$CeIrSnH_{0.7}$.[67]

Conclusion

Small hydrogen sorption in the Kondo semiconductor CeRhSb results in the 3.6(2) K antiferromagnet $CeRhSbH_{0.2}$. Both compounds adopt TiNiSi-related structures, but $CeRhSbH_{0.2}$ has the slightly higher cell volume. Resistivity and specific heat studies point to a considerable Kondo effect in the hydride. ^{121}Sb Mössbauer spectra are indicative for a slightly higher s-electron density at the antimony nuclei in $CeRhSbH_{0.2}$.

Acknowledgment. This work was financially supported by the Deutsche Forschungsgemeinschaft. B.C. and R.P. are indebted to the EGIDE and DAAD for research grants within the Procope programs (Grants 11457RD and D/0502176). Finally, B.C. thanks the European Science Foundation (ECOM-_COST action P16) for financial support.

Supporting Information Available: Crystallographic information (CIF). This material is available free of charge via the Internet at http://pubs.acs.org.

CM062168A

(61) Takabatake, T.; Tanaka, H.; Bando, Y.; Fuji, H.; Nishigori, S.; Suzuki, T.; Fujita, T.; Kido, G. *Phys. Rev. B* **1994**, *50*, 623.
(62) Nishigori, S.; Goshima, H.; Suzuki, T.; Fujita, T.; Nakamoto, G.; Tanaka, H.; Takabatake, T.; Fuji, H. *J. Phys. Soc. Jpn.* **1996**, *65*, 2614.
(63) Lloret, B.; Chevalier, B.; Buffat, B.; Etourneau, J.; Quezel, S.; Lamharrar, A.; Rossat-Mignod, J.; Calemczuk, R.; Bonjour, E. *J. Magn. Magn. Mater*. **1987**, *63*−*64*, 85.
(64) Calemczuk, R.; Bonjour, E.; Rossat-Mignod, J.; Chevalier, B. *J. Magn. Magn. Mater*. **1990**, *90*−*91*, 477.
(65) Mishra, R.; Pöttgen, R.; Hoffmann, R.-D.; Fickenscher, Th.; Eschen, M.; Trill, H.; Mosel, B. D. *Z. Naturforsch.* **2002**, *57b*, 1215.
(66) Lippens, P. E. *Solid State Commun.* **2000**, *113*, 399.
(67) Chevalier, B.; Sebastian, C. P.; Pöttgen, R. *Solid State Sci.* **2006**, *8*, 1000.